Self-trapping of a light particle in a dense fluid: Application of scaled density-functional theory to the decay of orthopositronium

Terrence Reese and Bruce N. Miller
Physics Department, Texas Christian University, Fort Worth, Texas 76129
(Received 17 January 1990; revised manuscript received 19 June 1990)

The localization of a light particle (e.g., electron, positron, or positronium atom) in a fluid is known as self-trapping. In an earlier paper [B. N. Miller and T. L. Reese, Phys. Rev. A **39**, 4735 (1989)] we showed that (1) the density-functional theories (DFT's) of self-trapping could be derived from a mesoscopic model that employs a quantum-mechanical description of the light particle and a classical description of the fluid, and (2) the application of scaling to the simplest variant of DFT results in a universal model for all fluids that obey the principle of corresponding states. In this paper we apply the fully scaled theory to the pickoff annihilation of orthopositronium. Predictions of three different versions of the theory are compared with the experimental measurements of McNutt and Sharma on ethane [J. Chem. Phys. **68**, 130 (1978)] and Tuomisaari, Rytsola, and Hautojarvi on argon [Phys. Lett. **112A**, 279 (1988)]. Best agreement is obtained from a model that incorporates transitions between localized and extended states.

I. INTRODUCTION

Experimental studies of the behavior of a light particle (electron, positron, or positronium atom) in a dense fluid indicate that, in certain regions of mean fluid temperature and pressure, the light particle alters the local fluid density in its vicinity. This alteration results in decreased mobility of the electron under the influence of an electric field,[1] a decrease in the decay rate of orthopositronium (ortho-Ps), or an increase in the decay rate of the positron.[2] The accepted explanation for this phenomena is that the light particle (hereafter LP) becomes localized in a semimacroscopic volume of altered fluid density that results from the interaction of the LP and fluid atoms or molecules. This localization process is referred to as self-trapping because the LP induces the formation of the potential well in which it is stabilized.[2]

The earliest theoretical models assumed that the trapped LP created either a bubble or droplet of constant density in the fluid, depending on whether the average interaction of the LP with a fluid atom or molecule was attractive (e.g., a positron) or repulsive (e.g., ortho-Ps).[2,3] These models were later defined via density-functional theory (DFT), in which a free energy Φ is constructed which is a functional of the mean local fluid density ρ and LP wave function ψ.[2,4-8] Coupled equations governing ρ and ψ are obtained from a variational principle by assuming that the best choices for ρ and ψ minimize Φ. Because DFT is a semimacroscopic model, it is not constructed from first principles. Realizations of DFT vary, in part, in the degree to which nonlocal correlations are taken into account. In DFT both localized and extended (propagating) solutions may be possible, depending on the temperature and average fluid density. DFT was used successfully by Stott and Zaremba[4] to interpret measurements by Hautojarvi *et al.* of the annihilation rate of positrons in He at low temperatures.[9]

A number of experimental groups have investigated the annihilation of positrons and orthopositronium in a variety of gases at higher temperatures.[10-14] In some cases, variants of DFT were used to analyze the data with varying success. The complexity of the models varied, and the approximation methods were not always clearly explained. Whether DFT can be used successfully to explain the new experiments is an open question and the central subject of this work.

In an earlier paper we introduced a mesoscopic model of the LP-fluid system in which the partition function is represented by a path integral with a state space density which depends explicitly on the LP wave function.[15] We showed that most DFT's could be derived from this model by selecting the ρ and ψ which optimize the measure in state space. We applied critical point scaling to the simplest resulting variant of DFT and showed that the coupled equations governing the wave function and local density were universal for all gases which satisfy the principle of corresponding states. A consequence of scaling is that all of the system specific constants can be lumped into a single dimensionless parameter which uniquely determines the properties of the localized state. We developed a numerical algorithm for solving the nonlinear coupled equations for ρ and ψ from a knowledge of the equation of state. As a simple test of the method, we used the van der Waals equation to show that the method could reproduce the qualitative features of experiments measuring the decay rate of ortho-Ps in gases.

In this paper we will thoroughly explore the possibility of using the fully scaled DFT to model the density and temperature dependence of experimental measurements of the decay rate of ortho-Ps in ethane and argon carried out by Sharma and co-workers,[10] and Tuomisaari, Rytsola, and Hautojarvi,[11] respectively. We will consider and critique three interpretations of the role of the semimacroscopic localized ground state discussed in the litera-

ture: (1) Following most theorists,[4–6] we will assume that the LP only exists in this state (referred to below as I1); (2) following Niemenen *et al.*,[7] we will assume that the observed decay rate can be computed from its thermal average, with contributions from both localized and extended states (referred to as I2); (3) following suggestions by Kowalski, Miller, and Percus,[16–18] we will assume that the LP undergoes transitions between the two types of states, and determine the longest characteristic time which governs the exponential decay of each mode (referred to as I3). We will demonstrate that while the first two "traditional" interpretations do not successfully reproduce the data, substantial improvements are obtained from the third. We will see that this conclusion is not surprising as the last case has the strongest physical basis. The first case can be regarded as a subset of the last if the transition probabilities are negligible, whereas the second case arises if the transition rates are extremely large. In carrying out the calculations we will employ realistic equations of state to model the fluids. We will explore the sensitivity of the predicted decay rates to the details of the equation of state by performing similar calculations with the van der Waals equation and comparing them with the realistic version.

This paper is divided into seven sections. The environment of the LP-fluid molecule system is described in Sec. II and the significance of the decay rate as a signature of localization is explained. The principles and equations of the fully scaled DFT are outlined in Sec. III and the details of the numerical methods required for their solution are described in Sec. IV. The two-state model is introduced in Sec. V, where the dependence of experimental measurements on the transition rates is developed. The results of fitting the three interpretations of DFT to experimental measurements of the annihilation rate of ortho-Ps in argon and ethane are presented in Sec. VI as well as a study of the possible benefits which arise from using a realistic equation of state. We conclude with a critique of DFT and a discussion of alternative models in Sec. VII.

II. ENVIRONMENT

When a positron is injected into a fluid, it can either annihilate with an electron provided by a fluid molecule, or it can combine with a free electron to form a positronium atom. Ps, which shares many of its characteristics with hydrogen, has two forms: parapositronium, with a singlet spin state, and orthopositronium, with a triplet spin state. Para-Ps decays via a 2γ process and has a vacuum lifetime of 1.45×10^{-10} sec, whereas ortho-Ps, since it requires a 3γ decay process, has a much longer lifetime, 1.45×10^{-7} sec. Due to the difference in vacuum lifetimes, after approximately 10^{-9} sec the probability of finding a surviving para-Ps atom is small and only orthp-Ps may be observed. Because of its long natural lifetime, the chief mode of decay of ortho-Ps is pickoff annihilation, whereby the positron decays with an electron from the valence shell of one of the fluid molecules. In the remainder of the paper references to Ps should be inferred to mean ortho-Ps.

A Ps atom in a dense fluid near its liquid-vapor critical point has a de Broglie wavelength much greater than the mean separation between the molecules of the fluid. This allows the Ps atom to interact with many fluid atoms at the same time. The interaction between the Ps atom and the fluid molecules is repulsive over short distances because of the fermionic repulsion between the electron of the Ps atom and the electrons of the fluid molecules. The combination of long de Broglie wavelength and short-range repulsion suggests that the Ps atom will attempt to create a region of low density around itself. The Ps atom may become trapped in this volume. For ranges of temperature and average density where the absolute value of the decrease in free energy caused by the formation of this region of low density is greater than the increase in free energy due to the pressure-volume work required to create it, the self-trapped state will become stable.[2,19]

The major change in the Ps-fluid molecule system caused by the formation of the self-trapped state is the large decrease in the number of fluid molecules near the Ps atom. In attempting to detect the self-trapped state the most straightforward course is to make measurements of quantities that are dependent on the local fluid density. The decay rate is an obvious choice because the annihilation rate of the positron is dependent upon the density of electrons in its vicinity. Figure 1 is a plot of the decay rate of Ps versus average density on various isotherms in ethane.[10] The straight line represents the decay rate of Ps in the absence of interaction between the Ps atom and the ethane molecules. It is apparent that the decay rate of each isotherm fails to keep up with the linear extrapolation. This deviation becomes more pronounced as the critical temperature is approached. Most of these isotherms can be split into three regions: (1) The transition region, where an isotherm just begins to diverge from the linear extrapolation. It continues until the curve starts to flatten out and form a plateau. (2) A region consisting of the plateau and part of the upswing of the curve that follows. In the semimacroscopic

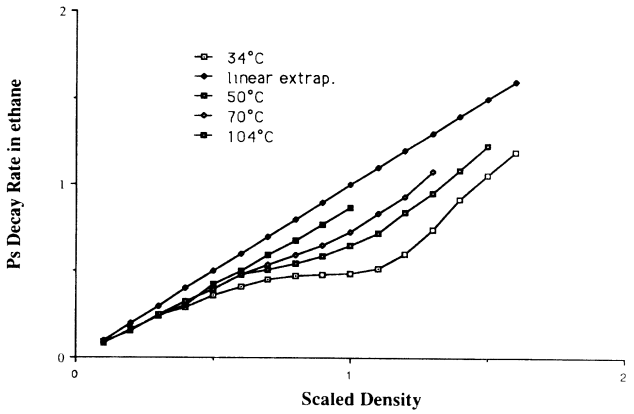

FIG. 1. A plot of the decay rate of ortho-Ps vs density in ethane on the isotherms $T=34$, 50, 70, and 104 °C. The linear extrapolation represents the decay rate of ortho-Ps in the absence of interaction between the LP and the fluid molecules. The data was taken from experiments done by Sharma and coworkers (Ref. 10). All of the units are dimensionless.

language of DFT, we infer that here self-trapping predominates. This is the region of greatest theoretical interest. (3) A region where the isotherm rejoins the linear curve and the self-trapped state collapses completely.

III. MESOSCOPIC MODEL

The mesoscopic model was created as an attempt to understand the self-trapped state at a more fundamental level than DFT.[15] The model treats the LP degrees of freedom by quantum mechanics and the fluid-molecule degrees of freedom classically. It allows the LP and the fluid molecules to interact self-consistently and takes into account the large isothermal compressibility of the fluid near the liquid-vapor critical point.

The canonical partition function Z_N representing the LP-fluid molecule system is given by the functional integral

$$Z_N=(1/\Lambda_{\rm th})^{3N}\int D_\psi\delta(\langle\psi|\psi\rangle-1)\times\exp(-\beta\langle\psi|\hat{P}^2/2m|\psi\rangle)Q_{CN}(\psi)$$
$$=(1/\Lambda_{\rm th})^{3N}\int D_\psi\delta(\langle\psi|\psi\rangle-1)\exp(-\beta\Phi_N)\ , \qquad (1)$$

where $\hat{P}\equiv(\hbar/i)\nabla$, $\Lambda_{\rm th}$ is the molecular thermal wavelength $[h/(2MkT)^{1/2}]$, and $Q_{CN}(\psi)$ is the configurational partition function of a fluid experiencing a nonuniform potential. The δ function assures that only normalized wave functions contribute. From (1) it is clear that Φ_N is a minimum for the most probable states.

If we nullify the variation of the density functional Φ_N with respect to the LP wave function and the local fluid density and assume that the optimal LP wave function varies slowly over distances on the order of the mean separation between the fluid molecules, we obtain two coupled equations relating the LP wave function and local fluid density. Further, if we assume that the LP-fluid molecule interaction can be described by a Fermi pseudopotential and scale the resulting coupled equations by the steps outlined in our previous paper[15] (Sec. III A), they take the dimensionless form

$$(-\Delta_x+\hat{\rho})\varphi=\varepsilon\varphi\ , \qquad (2)$$

$$|\varphi|^2=\beta(\mu_0-\mu)\ , \qquad (3)$$

where the scaled position, density, wave function, and energy are defined as $\mathbf{x}=a\mathbf{r}$, $a=[2mc\rho_0/\hbar^2]^{1/2}$, $\hat{\rho}=\rho/\rho_0$, $|\varphi|^2=\beta c|\psi|^2$, and $\varepsilon=E/c\rho_0$, respectively. μ is the local chemical potential and c is the Fermi pseudopotential interaction strength. Quantities with a subscripted zero represent their value at a distance sufficiently far away from the LP to guarantee that it has no effect on the fluid density. According to the principle of corresponding states,[20] $\beta\mu$ is a universal function of the reduced thermodynamic variables $\rho'\equiv\rho/\rho_c$ and $T'\equiv T/T_c$, where, as usual, the subscript c denotes the critical point. We are thus assured that solutions of (2) and (3) have the same form for a large number of elements and compounds. If we assume that the Ps wave function is spherically symmetric, then the coupled equations can be reduced to a single spatial dimension.

Equations (2) and (3) define a nonlinear eigenvalue equation for ε. The value of the scaled Lagrange multiplier ε is fixed by the condition $\langle\psi|\psi\rangle=1$. In terms of scaled quantities this condition takes the form

$$I_n(\varepsilon)=(1/4\pi)\int|\varphi|^2d\mathbf{x}$$
$$=(\rho')^{3/2}(4\pi)^{1/2}[(\lambda_c)^2(L_s)^{5/2}/(l_c)^{9/2}]/T'$$
$$=(\rho')^{3/2}\Lambda/T'\ . \qquad (4)$$

The value of $I_n(\varepsilon)$, the normalization integral of the scaled wave function, is therefore determined by three characteristic lengths: the scattering length of the Ps-atom–fluid-molecule interaction (L_s), the thermal wavelength of Ps at the critical temperature (λ_c), and the mean separation between the fluid molecules at the critical density (l_c). All system specific parameters required for the solution of the coupled equations appear only in the universal constant Λ.

From the first law of thermodynamics the difference in chemical potential, which appears on the right-hand side of (3), is given by

$$\mu_0-\mu=-\int_{\rho_0}^{\rho}d\rho''(1/\rho'')(\partial P/\partial\rho'')\ , \qquad (5)$$

where P is the hydrostatic pressure. Thus its determination depends upon the equation of state selected. In our earlier paper we used the van der Waals equation of state to simulate the fluid.

IV. METHOD OF CALCULATION

An algorithm was created to solve the coupled equations (2) and (3) and calculate five important properties of the self-trapped state. These are the scaled normalization integral, total LP energy, Helmholtz free energy, number of fluid molecules displaced by the formation of the trap, and the pickoff decay rate. The scaled energy is taken as an input, and then calculated directly in terms of φ as a consistency check on the method. In order to determine ρ from a given value of φ, the algorithm creates a lookup table of values that relates the local fluid density to the square of the wave function through (3). The value of the wave function at the origin is selected and a combination of the fourth-order Runge-Kutta and Adams-Bashforth codes is used to determine its dependence on the radial coordinate. Since the shape of the ground-state wave function is unimodal, the iteration can be combined with a simple bisection routine to converge to the correct initial value of the wave function to within a factor of 10^{-6}.

The five properties of interest only depend on the wave function and local fluid density which are determined by the algorithm for a given mean fluid temperature and density. The two most important quantities for the purpose of comparison with experimental data are the Helmholtz free energy and the decay rate. The free energy is used to determine the relative stability of localized versus extended states. The scaled versions of the decay rate and free energy, which are computed by the algorithm, are given by

$$\Phi/c\rho_0=\varepsilon-1+(1/I_n)\int_0^\infty dx\, x^2[\beta P_0/\rho_0-(\beta P/\rho)\hat{\rho} -\beta(\mu_0-\mu)\hat{\rho}] , \quad (6)$$

$$\lambda_{po}/B\rho_0=(1/I_n)\int_0^\infty dx\, x^2\hat{\rho}\varphi^2 , \quad (7)$$

where Φ and λ_{po} are the Helmholtz free energy and pickoff decay rate before scaling, and B is a constant derived from quantum field theory.

The only quantities required as input for the calculations are the reduced density and temperature, ρ' and T', and the scaled energy, ε. Since the interaction of the LP with the surrounding medium is repulsive, the condition that φ vanishes at ∞ and has finite norm restricts ε to the unit interval. This energy range is partitioned into 100 equal regions. For each T', calculations were carried out in the density region corresponding to $0<\rho'<3.0$ in increments of 0.1. The limits on the range of values for the density and temperature were determined by the equation of state.

The algorithm is used to numerically solve the two coupled equations (2) and (3) and calculate scaled values for the five quantities mentioned above for each ε $(0<\varepsilon<1)$ at a specific ρ' and T'. We then compare the normalization integral for each ε with $(\rho')^{3/2}\Lambda/T'$. When the two sides are equal, a self-trapped solution exists for this particular ε at the given density and temperature. The desired values of the remaining (four) properties are then determined from the appropriate ε. Since the critical density of a particular fluid and the critical wavelength of the LP are known quantities, variations in Λ reflect different possible values for the Ps–fluid-molecule scattering length which affects the depth of the trapped state and the length of the trapping region.

Although no reliable experimental data on the Ps–fluid-molecule scattering length exists, it can be estimated by considering molecular geometries and calculating the distances between the respective centers of mass of the Ps atom and the fluid molecules. This calculation requires estimates of the size of the Ps atom and the fluid molecules and a knowledge of the structure and possible orientations in space of the fluid molecule. If one assumes that Ps has a radius of 0.5 Å and that argon has a diameter of 1.4 Å, then the Ps–fluid-molecule scattering length can be estimated as 1.2 Å, which gives $\Lambda=12.84$. If one assumes that the carbon atom has a diameter of 2 Å and hydrogen has a diameter of 1 Å, then the Ps–fluid-molecule scattering length is approximately 3 or 2.46 Å, depending on the orientation of the ethane molecule, which gives the Λ values 9.46 and 5.879, respectively. Note that, in computing Λ, the scattering length is raised to the 5/2 power. Consequently, small differences in the scattering length result in large differences in Λ.

The decay rates and free energies computed with the algorithm are scaled $[0<\lambda_{po}/(B\rho_0)<1, \quad -1<\Phi/(c\rho_0)<1]$ and must be converted to unscaled but still dimensionless values. The predicted decay rates can then be plotted versus the average fluid density on isotherms to compare with experimental data.

V. METHODS OF INTERPRETATION

To date, two models have proved popular for converting the scaled decay rate into a useful value for comparisons with experiment. We will discuss the underlying motivation for each of them, and then introduce a third model which we believe has the strongest physical basis. In the first, and most straightforward, it is assumed that the contribution to λ arises solely from the trapped state. Since Eqs. (2) and (3) admit to both trapped and free (extended) solutions it may seem surprising to single out only the localized contribution to λ. This suggests that when trapping occurs, the extended state is simply not populated to any appreciable degree. From statistical mechanics, the probability ratio for trapped and extended states is given, in an obvious notation, by $p_t/p_e=\exp(-\Phi)$, where Φ is simply the difference in free energy between the two states. It would seem that Φ could be easily computed by substituting the appropriate solutions for each state in (5) along with the usual local thermodynamic approximation.[15] However, in solving the governing equations (2) and (3) for the spherically symmetric trapped ground state, we anchored the LP center of mass at the origin. Thus we broke translational symmetry and ignored the contribution to Φ from diffusive (or ballistic) motion of the trap as a whole. While it is not expected that the inclusion of kinetic effects will strongly alter the average density profile or wave function, it will surely increase the entropy and decrease the free energy, further stabilizing this state. Some time ago Gersch estimated the effective mass of an electron trap in an ideal gas and showed that drift can substantially increase the entropy.[21] These results *suggest* that, when it exists, the trapped state may be dominant.

To compare the calculations with data, we merely reverse the scaling we carried out earlier by multiplying the left-hand side of (7) by ρ', and set B equal to 1. Since B is a quantity derived from field theory, setting B equal to 1 is equivalent to setting the slope of the linear extrapolation equal to 1.

The second method used for conversion was introduced by Nieminen *et al.*[7] and calculates the thermally weighted mean of the decay rate,

$$\lambda/\rho_c=(\rho' e^{\beta\Phi}+\lambda_p)/(1+e^{\beta\Phi}) , \quad (8)$$

where Φ is computed from (5) and the ground-state solutions of (2) and (3) without the kinetic contributions discussed above, and λ_p is the scaled decay rate calculated by the algorithm multiplied by ρ', $\lambda_p=(\rho'/I_n)\int x^2\varphi^2\hat{\rho}\,dx$. This model has the apparent virtue of converging on λ_e, the decay rate associated with extended states, at the extremes of the trapping region where $\beta\Phi\gg1$. In contrast with the first interpretation, the thermal average of λ represents the physical observable in the opposite extreme where transition rates between the two states (extended and trapped) are much greater than the annihilation rate in either pure state.

The physical experiment measures the attenuation of the mean population of positrons in the fluid with time. The third model, which we introduce here, also uses the two-state model to calculate the decay rate of the system.

However, it directly takes into account possible transitions of the LP between the states as time progresses. If the LP undergoes transitions between two states, say A and B, and the transition process is Markovian, then the probability of finding the LP in either state is governed by

$$\frac{dP_A}{dt} = -(\lambda_A + C_{BA})P_A + C_{AB}P_B \ , \tag{9}$$

$$\frac{dP_B}{dt} = C_{BA}P_A - (\lambda_B + C_{AB})P_B \ , \tag{10}$$

where λ_A and λ_B are the annihilation rates of the pure states, C_{BA} is the transition rate from state A to B and vice versa for C_{AB}. Equations (9) and (10) comprise a linear eigenvalue problem with the following solutions for P_A and P_B:

$$\begin{aligned} P_A &= A_1\exp(-\lambda_1 t) + A_2\exp(-\lambda_2 t) \ , \\ P_B &= B_1\exp(-\lambda_1 t) + B_2\exp(-\lambda_2 t) \ . \end{aligned} \tag{11}$$

The eigenvalues λ_1 and λ_2 can be expressed in terms of the transition rates and decay rates by

$$\lambda_1 = (\lambda_A + \lambda_B)/2 - (p/2)\{1 - [1 + 2q(\lambda_A - \lambda_B)/p^2 + (\lambda_A - \lambda_B)^2/p^2]^{1/2}\} \ , \tag{12}$$

$$\lambda_2 = (\lambda_A + \lambda_B)/2 - (p/2)\{1 + [1 + 2q(\lambda_A - \lambda_B)/p^2 + (\lambda_A - \lambda_B)^2/(p^2)]^{1/2}\} \ , \tag{13}$$

where

$$p = C_{AB} + C_{BA}, \quad q = C_{BA} - C_{AB} \ . \tag{14}$$

λ_1 and λ_2 represent the *experimentally observed* decay rates, and t is the time elapsed since the beginning of the experiment (the instant of positronium formation). In this notation A and B refer to the trapped and free states of the system, respectively.

In principle, from detailed balance, the ratio of the transition rates is given by $\exp(-\beta\Phi)$. In practice, this ratio is difficult to compute because it requires the inclusion of kinetic effects (see above) in addition to the configurational free energy which depends on φ and ρ. Detailed balance does not provide the actual numerical value of each transition rate. Thus, at present, we must treat them as adjustable parameters.

Most experiments measure λ_2, the inverse lifetime of the mode with greatest longevity. In terms of the quantities calculated by the numerical algorithm, (12) becomes

$$\lambda_2 = (\lambda_p + \rho')/2 - (p/2)\{1 + [(\rho' - \lambda_p)^2/p^2 + 2q(\rho' - \lambda_p)/p^2 + 1]^{1/2}\} \ . \tag{15}$$

With a little algebra it is easy to show that (15) reduces to λ_p when both q and p are small ($p, q \ll \lambda_p$), and to (8) when p is large.

VI. RESULTS

In this section we compare the results of the model calculations discussed above with experimental measurements of the Ps decay rate in argon and ethane. We use both the modified Benedict-Webb-Ruben[22] (MBWR) and van der Waals equations of state to model the fluids. The data are taken from the experiments of Sharma and coworkers[10] and Tuomisaari, Rytsola, and Hautojarvi[11] which measure the decay rate of Ps in ethane at 307.15, 323.15, and 343.15 K and in argon at 160 and 200 K and plot them against the average fluid density.

In contrast with the theoretical values, most experimental reduced densities and temperatures will not be integer multiples of 0.1. We addressed this problem by using the interpolated curves provided by the experimentalists as data points. We chose values of the decay rate on the curves which corresponded to our values of ρ'. Because the interpolations are simply best fits to actual data, this choice may introduce some error. However, compared to the differences with the theoretical curves, it is small.

To obtain data points from the plots, a fine Cartesian grid was laid over the experimental plots and the coordinates of the desired density points were recorded. In these plots, the nonzero intercept at zero density is simply the vacuum decay rate of ortho-Ps. It must be taken into account when taking readings, since it does not contribute to the pickoff decay rate computed from theory. To obtain a dimensionless decay rate from the data and to minimize any problems arising from instrument calibration, the actual value used was λ/λ_0, where λ is the difference between the vertical component of the isotherm above the density axis and the vacuum decay rate, and λ_0 is the difference between the vertical component of the linear extrapolation and the vacuum decay rate. The value of λ/λ_0 can be stored and used for comparisons. Since λ_0 is proportional to ρ', when these values are replotted they must be multiplied by the scaled density ρ' to obtain a graph of λ versus ρ' with the correct shape.

It was pointed out in Sec. V that even an approximately complete theory of the transition rates does not exist. In order to implement I3 we have made the simplifying assumption that C_{AB} and C_{BA} depend only on temperature. This obviously leads to problems near the critical isotherm, where deeply trapped states are highly favored for reduced densities near unity, while extended states are favored at the extremes of low and high density. However, for reduced temperatures at least a few percentage points above unity, the assumption is more reasonable. The theoretical results were obtained by calculating the decay rate from (15) for integer values of Λ, C_{AB}, and C_{BA} and performing a least-squares fit to the experimental data. Choosing parameter values with smaller increments did not materially affect the outcome.

The presentation of the results is divided into three sec-

tions: In Sec. VI A theory and experiment are compared on isotherms for different values of Λ. In Sec. VI B theoretical results for ethane and argon are compared for the same values of Λ as a check on scaling. In Sec. VI C differences between the calculations given by the MBWR equation of state and those given by the van der Waals equation using I1 are described.

A. Comparisons with experiments

Assuming that only the trapped state contributes (I1) to the decay rate, plots of the theoretical decay rate for ethane are presented in Figs. 2(a) and 2(b) at 34 and 50 °C with Λ values of 2.0, 3.0, and 4.0 using the MBWR equation of state. The experimental data are also displayed as well as the linear, low-density extrapolation. It is obvious that the theoretical and experimental curves have very little in common. While the experimental curves for all the isotherms are for the most part monotonically increasing, the theoretical curves are concave upward. At the lowest density where the theoretical self-trapped state exists, the experimental data suggest "deeper" trapping than the theory. However, following a small increment in density, the pattern reverses and the two curves diverge rapidly. Increases in temperature tend to increase the divergence between the curves, which means that a higher Λ value is required to maintain a point of intersection between them.

The minimum of the decay rate of the theoretical curves, which represents the average density at which the Ps atom is most deeply trapped, occurs between $\rho' = 1.3$ and 1.4 for all isotherms. Increases in temperature result in the theoretical isotherms' becoming more symmetrical about this minimum value.

From Fig. 1 we notice that the isotherm $T = 104$ °C has a slightly lower decay rate than the linear extrapolation. In our calculations we were never able to find a trapped state for this temperature no matter how much Λ was lowered. We were also never able to discover any trapped states for $\Lambda = 1.0$.

The theoretical results for the decay rate of Ps in ethane for the two-state model with transitions (I3) are plotted in Figs. 3(a) and 3(b). $\Lambda = 5 (L_s = 2.3$ Å), and

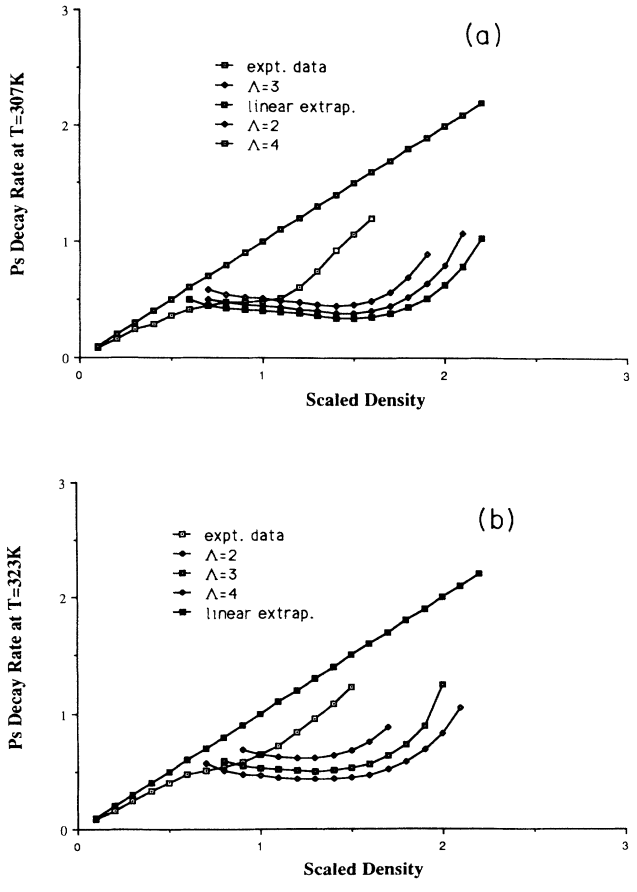

FIG. 2. (a) A plot of the theoretically calculated decay rate of ortho-Ps vs density in ethane at $T = 34$ °C for I1. The values of the universal constant (Λ) are 2.0, 3.0, and 4.0. The experimental data and the linear extrapolation are included. (b) A plot of the theoretically calculated decay rate of ortho-Ps vs density in ethane at $T = 50$ °C for I1. The values of the universal constant (Λ) are 2.0, 3.0, and 4.0.

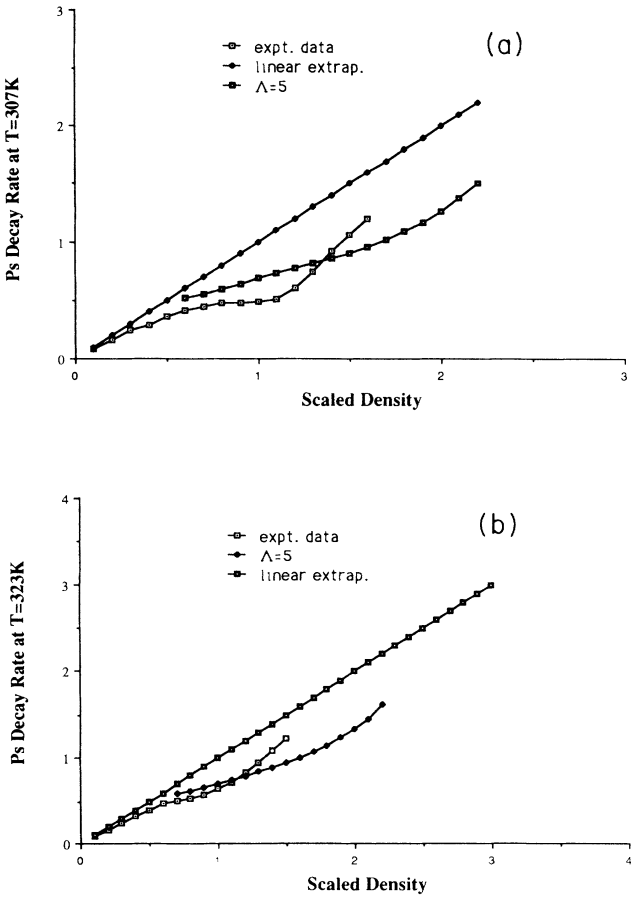

FIG. 3. (a) A plot of the theoretically calculated decay rate of ortho-Ps in ethane at $T = 34$ °C for I3. A Λ value was determined from a least-squares fit for Λ and the transition rates. (b) A plot of the theoretically calculated decay rate of ortho-Ps in ethane at $T = 50$ °C for I3.

$C_{AB}=1$, and $C_{BA}=2$ gave the best fit to the experimental data for ethane.

Figure 3(a) is a plot of the theoretical decay rate, using I3, and the experimental decay rate of Ps in ethane at 34 °C. This is less than 1 °C above the critical temperature. The experimental curves were provided by Sharma.[10] The linear extrapolation is also displayed on the graphs to make the comparisons with the experiments easier. For each temperature the transition model I3 gave a curve which was monotonically increasing, whereas at 34 °C the experimental data have a plateau occurring approximately in the region around $\rho' \approx 1.1$. The theoretical prediction is higher than the experimental data in the density range $0.6 < \rho' < 1.2$. After $\rho' = 1.1$ the experimental curve's slope rapidly increases and, before $\rho' = 1.3$, overtakes the theoretical plot, which continues to gently slope upward.

Figure 3(b) is similar to Fig. 3(a), but the temperature is 50 °C. This curve and other theoretical curves at higher temperatures more closely resemble the experiments than Fig. 3(a). This is as expected because the assumption of density-independent transition rates is more reasonable away from the critical temperature. They exhibit the same tendencies as Fig. 3(a), but to a lesser degree. In all theoretical results to date, for ethane, the theoretical curves calculated using I3 have a trapping region that is much longer than the experimental curve. This added region was purposely omitted when the least-square distance algorithm was performed.

Figures 4(a) and 4(b) consider the same experimental data as Figs. 3(a) and 3(b). However, in these plots the data are compared with the predictions of Nieminen's model (two states with thermal averaging, I2) instead of the transition model. The Λ values in Figs. 4(a) and 4(b) were the same as those in Figs. 3(a) and 3(b) and were not "reoptimized." Using different values for Λ did not improve the agreement. These plots show that, in contrast with the experimental curves, I2 has a pronounced minimum near $\rho' \approx 1.5$ followed by a rapid approach to the homogeneous environment.

Figures 5(a)–5(c) display the decay rate at 160 K in argon. Figure 5(a) compares the experimental data with a least-squares best fit curve using I3. $\Lambda=8$ (1.21 Å) gave the best fit for argon at both 160 and 200 K. Figures 5(b) and 5(c) are plots of the decay rate for the transition model (I3) and Nieminen's model (I2), respectively, using $\Lambda=4$, 10, and 20 to compare results for small (4), medium (10), and large (20) values of Λ. As in ethane, at the theoretical onset of trapping for I3, the predicted value is greater than the experimental measurements. The decay rate of the experimental curve eventually does increase faster and overtakes the theoretical curves. The plots also show that the smaller Λ, or the smaller the Ps–fluid-molecules scattering length, the greater the average density where the experimental and theoretical curves intersect. This indicates that the smaller Λ values produce larger slopes. Figure 5(c) gives a much better appreciation for how I2 changes with increasing Ps–fluid-molecule scattering length. Increases in Λ result in a wider plateau.

At 200 K only I3 was capable of giving an approximately linear function, like the experimental isotherm. Figure 6 shows this plot for $\Lambda=8$. From this plot one can see that at this temperature, which corresponds to $T' \approx 1.325$, the theoretical curve is linear and is extremely similar to the experimental curve over the theoretical region of trapping. Unfortunately the length of the theoretical trapping region is too small. It is almost half that of the experimental trapping region, depending on where one considers self-trapping to begin on the experimental curve. Increases in Λ result in an increase in the length of the trapping region and a decrease in the slope of the function.

B. A test of universality

As a test of universality, we compare the predictions of the single-state version (I1) for the different gases using the same values of Λ. Figure 7 presents trapped state calculations (I1) of the dimensionless decay rate (in scaled units) versus the average *reduced* density using the MBWR equations of state for ethane and argon at their respective liquid-vapor critical temperatures for $\Lambda=16$ and 8. The name of the molecule is attached to the end

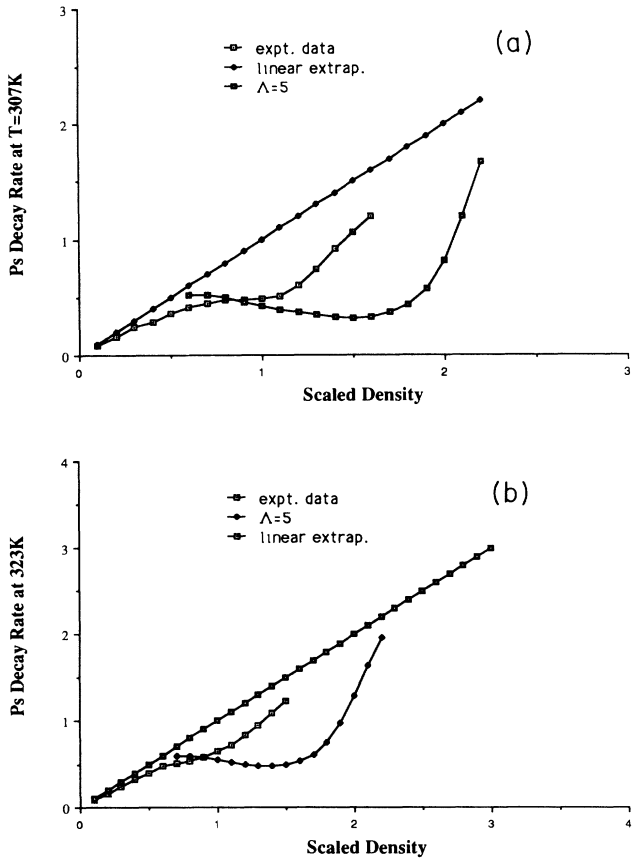

FIG. 4. (a) A plot of the theoretically calculated decay rate of ortho-Ps in ethane at $T=34$ °C for I2. The Λ value was maintained at 5.0 for comparative purposes. (b) A plot of the theoretically calculated decay rate of ortho-Ps in ethane at $T=50$ °C for I2.

of the appropriate Λ value, i.e., Λ=16ethane is defined as Λ=16 for the ethane molecule. The shape of the curves at the critical temperature for each Λ is nearly identical. The only difference is the length of the trapping region. The curves for each Λ value start out almost identically.

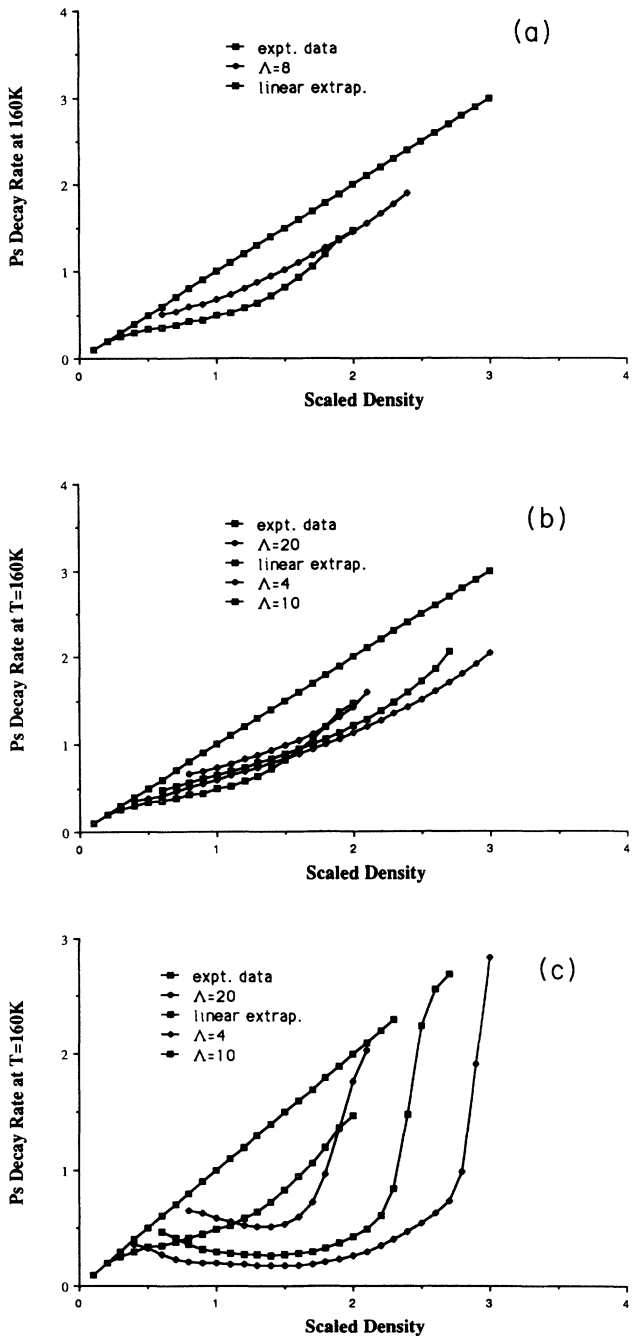

FIG. 5. (a) A plot of the theoretically calculated decay rate of ortho-Ps in argon at $T=160$ K for I3. The Λ value was determined from a best-fit solution. (b) A plot of the theoretically calculated decay rate of ortho-Ps in argon at $T=160$ K for I3. A large, medium, and small (20.0, 10.0, and 4.0) value of Λ were selected to examine how changes in the Λ value affected the isothermal curves. (c) A plot of the theoretically calculated decay rate of ortho-Ps in argon at $T=160$ K for I2.

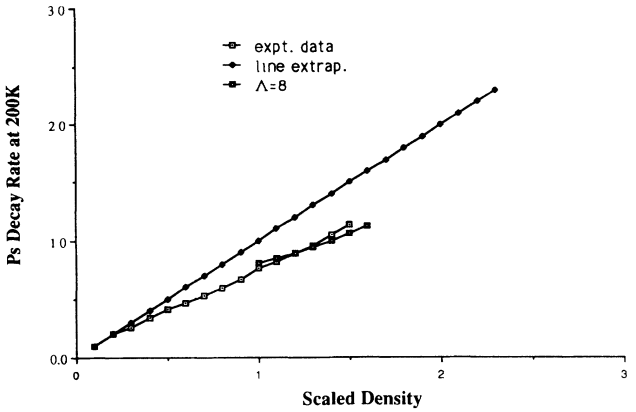

FIG. 6. A plot of the theoretically calculated decay rate of ortho-Ps in argon at $T=200$ K for I3. Only I3 was able to give a nearly linear curve for the decay rate.

However, toward the end of the trapping region, the decay rate in ethane increases slightly faster than the decay rate in argon. The small difference in behavior for different Λ values is the average density at which the decay rate for ethane and argon begin to diverge. At Λ=16 the two curves begin to diverge at $\rho'=1.9$.

Figure 8 is the same plot as those of Fig. 7 except at $T'=1.1$ and that Λ=4 has replaced Λ=16. For both Λ values the curves are nearly identical except at the last density point for Λ=8. On the other hand, for Λ=16, which is not shown, the decay rates begin to diverge much earlier. As in the preceding case, the ethane decay rate curve increases faster than that for argon toward the end of the trapping interval. Similar to the preceding results, increases in Λ result in a larger divergence between the theoretical decay rate curves of ethane and argon.

Figures 7 and 8 strongly support the assertion that the scaled DFT is universal. Ethane is a two-centered molecule with a nonvanishing quadrupole moment, whereas argon is spherically symmetric. Even though their equations of state are markedly different, if the same value of

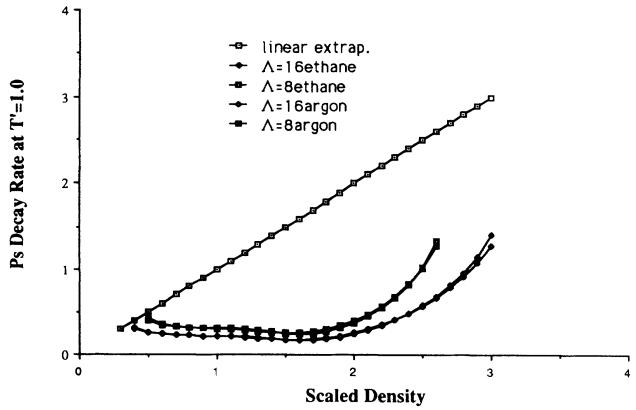

FIG. 7. A plot of the theoretically determined decay rate of ortho-Ps vs density at the liquid-vapor critical point, $T'=1.0$, for ethane and argon. The selected Λ values were 8.0 and 16.0.

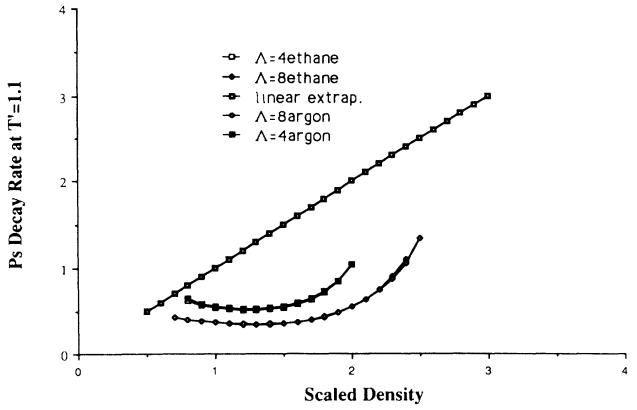

FIG. 8. A plot of the theoretically determined decay rate of ortho-Ps vs density at $T'=1.1$ for ethane and argon. The selected Λ values were 4.0 and 8.0.

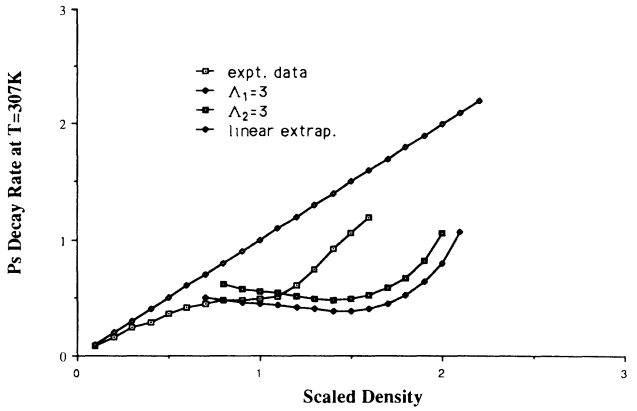

FIG. 9. The theoretically calculated rate of ortho-Ps in ethane at $T=34\,^{\circ}\mathrm{C}$ using the MBWR equation of state (Λ_1) and the van der Waals equation of state (Λ_2).

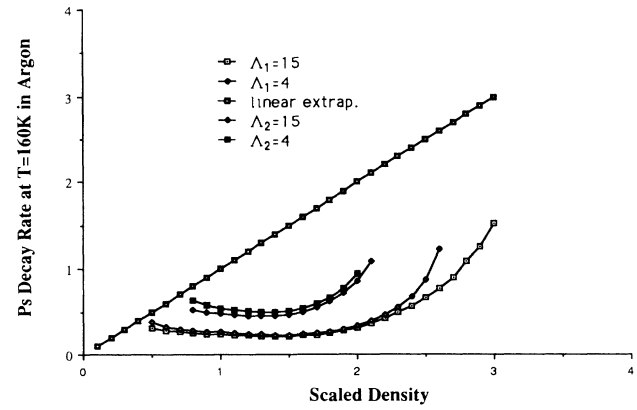

FIG. 10. The theoretically calculated decay rate of ortho-Ps in argon at $T=160$ K using the MBWR (Λ_1) and the van der Waals (Λ_2) equations of state.

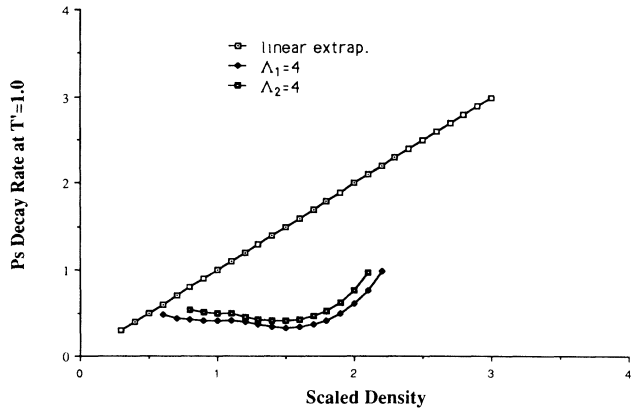

FIG. 11. The theoretically calculated decay rate of ortho-Ps in ethane at $T'=1.0$, using the MBWR equation of state (Λ_1) and the van der Waals equation of state (Λ_2).

Λ is selected, the solutions for $\varphi(r)$ and $\hat{\rho}(r)$ are very similar and yield nearly the same scaled observable.

C. Importance of the equation of state

Figures 9–11 compare the model predictions using model I1, for both the van der Waals and the MBWR equations of state. Figure 9 shows how the decay rate differs between the MBWR and the van der Waals equations of state for ethane. We follow the same procedure in Fig. 10 using argon as the comparison fluid at $T=160$ K. Figure 11 presents a similar comparison on the critical isotherm of ethane. In all three plots Λ_1 and Λ_2 represent the results for the MBWR and the van der Waals equations of state, respectively.

In Fig. 9 the theoretical results for the van der Waals equation show the same general relationship to the ethane experimental data as the MBWR results. The difference between the MBWR ethane curves and the van der Waals ethane curves is basically one of degree and concerns the depth of trapping and length of the trapping region. The same thing can be said for the curves in Fig. 10, in which the van der Waals is compared to the MBWR results for argon at $T=160$ K for $\Lambda=15$ and 4.

In all cases the localized ground state induced by the van der Waals equation turned out to be less deeply trapped than those induced by MBWR. The plots also indicate that decreases in the value of Λ decrease the divergence between the van der Waals and the MBWR results. Since the curves are so similar, it is obvious that changes in equation of state do not create radical changes in theoretical results for the DFT considered here.

VII. CONCLUSIONS

In our earlier paper we demonstrated that the simplest variant of DFT is universal and that, for this variant, there are only three system specific parameters (scattering length, mean molecular separation, and mean thermal wavelength at the critical point) which are all lumped in the single dimensionless constant Λ. We also found that DFT yielded qualitative agreement with experimental

measurements of the ortho-Ps decay rate in ethane for the simplest interpretation of the model (I1) using a crude equation of the state (van der Waals). This provided the motivation to extend the calculations by employing an extremely accurate equation of state (MBWR), and to investigate two additional methods for interpreting the model (I2 and I3), one of which (I3) seemed to us to be preferable physically.

The details of the calculations and comparison with experimental measurements of the ortho-Ps decay rate in argon and ethane lead to the following conclusions.

(1) The density range where DFT predicts the existence of trapped states depends on Λ. At each temperature there is a critical value, say Λ_c, below which stable trapping does not occur. The finite interval results in unphysical discontinuities in predicted observables at the end points. This effect is minimized whenever a thermal average is computed because the probability of trapping is reduced at the interval boundaries.

(2) The overall shape of plots of decay rate versus density contributed by the ground state (I1) is roughly similar for different values of Λ, but there is a large range for the minimum value, which decreases with increasing Λ.

(3) The simplest interpretation of the theoretical model (I1), where it is assumed that only the trapped state contributes to the decay rate, still provides only qualitative agreement with experiment. Theory and experiment both indicate that trapping is most prominent in a broad range of temperature and density near the liquid-vapor critical point, where the fluid is easily compressed. However, for ethane, the predicted density range for "deep" trapping is much larger than the observations suggest and, correspondingly, the predicted density where the trapping is strongest is too large. The available data for argon do not come sufficiently close to T_c to allow us to draw the same inference. At 160 K, the tendency appears to be the reverse of that for ethane, but the trapping is not nearly so pronounced.

(4) Much better quantitative agreement is obtained for each gas by assuming that transitions occur between trapped and extended states. In fact, this is the only version which predicts deviations from linearity at 200 K for argon. Because these calculations involve a three-parameter fit (scattering length, or Λ, C_{AB}, and C_{BA}) we expect it to be better. For the data considered, the only difficulty arises within one degree of the critical isotherm of ethane, where the assumption of density-independent transition rates is unreasonable.

(5) The numerical results indicate the Ps–fluid-molecule scattering length is 2.3 Å for ethane and 1.21 Å for argon. These results are within 6% of the earlier estimates of the scattering length, based solely on mean molecular size and bond length.

(6) It is surprising that the MBWR and the van der Waals equations of state result in predictions that are not only qualitatively similar, but quantitatively close except near the right-hand side of the trapping interval. From Eq. (5) it is clear that the isothermal compressibility is the chief determinant of the coupled equations. We anticipated that choosing equations with different, more realistic, compressibilities would have a strong effect on the predictions. This is not the case.

The two essential difficulties faced by the scaled DFT are (1) it is a mean-field theory and hence ignores the contribution fluctuations and (2) it turns on and off at specific densities, resulting in discontinuous observables. In our earlier paper[15] we showed that DFT can be derived from a field theory with Hilbert-space measure $\delta(\langle\psi|\psi\rangle-1)\exp(-\beta\Phi)$. In an attempt to eliminate the main disadvantages of DFT, Fan and Miller recently employed this measure directly to compute the decay rate of ortho-Ps in the transition region of argon.[22] They included all contributions from a family of spherically symmetric wave functions depending on one parameter. Good agreement was obtained, but at a price: it was necessary to artificially limit the variance of the wave-function family considered. Calculations carried out by Silli, Tuomisaari, and Niemenen in a similar vein required artificial limitations on the spatial extent of *density* fluctuations.[23] In each case, the source of these problems appears to be the imposed breaking of translational invariance which results from fixing the center of symmetry of the family of contributing fluctuations. In principle, artificial symmetry breaking can be avoided in the complete mesoscopic model.[15] It is also avoided in the path-integral representation of a light particle first introduced in the study of the polaron by Feynman,[24] and later applied to the solvated electron by Chandler and coworkers,[25] Berne,[26] and others.

Important questions concern the relationship between these models, and their use for computing the observable properties of localized positrons and positronium. Miller and Fan have studied these questions very recently.[27] They have shown that the ortho-Ps pickoff decay rate depends sensitively on the behavior of the LP-fluid correlation function at short distances (on the order of an angstrom). It is not surprising that DFT has difficulty reproducing the experimental data, since it is semimacroscopic and represents the complete LP-fluid interaction with a single parameter, the scattering length. It will be interesting to learn if predictive as well as conceptual benefits from the Monte Carlo computations are forthcoming or if further improvements in mean-field theory are possible.

ACKNOWLEDGMENTS

We benefited from conversations with J. Percus, J. Kowalski, Y. Fan, and S. C. Sharma. We are grateful for the plots of experimental data for ethane supplied by S. C. Sharma and the program for generating the MBWR equation of state provided by J. Ely. We wish to acknowledge the support of the Robert A. Welch Foundation of Houston, Texas through Grant No. P-1002 and the Research Foundation of Texas Christian University through Grant No. 5-23112.

[1]N. Gee and G. R. Freeman, Can. J. Chem. **64** 1810 (1986).
[2]I. T. Iakubov and A. G. Khrapak, Prog. Phys. **45**, 697 (1982).
[3]J. L. Levine and T. M. Sanders, Phys. Rev. **154**, 138 (1967).
[4]M. J. Stott and E. Zaremba, Phys. Rev. Lett. **38**, 1493 (1977).
[5]C. Ebner and C. Punyanita, Phys. Rev. A **19**, 856 (1979).
[6]R. L. Moore, C. L. Cleveland, and H. A. Gersch, Phys. Rev. B **18**, 1183 (1978).
[7]R. M. Nieminen, M. Manninen, I. Välimaa, and P. Hautojarvi, Phys. Rev. A **21**, 1677 (1980).
[8]J. P. Hernandez, Phys. Rev. B **11**, 1289 (1975).
[9]P. Hautojarvi, K. Rytsola, P. Tuovinen, A. Vehanen, and P. Jauho, Phys. Rev. Lett. **38**, 842 (1977).
[10]S. C. Sharma, R. H. Arganbright, and M. H. Ward, J. Phys. B **20**, 867 (1987); S. C. Sharma and E. H. Juenguman, Phys. Lett. A **144**, 47 (1986).
[11]M. Tuomisaari, K. Rytsola, and P. Hautojarvi, Phys. Lett. **112A**, 279 (1988).
[12]J. D. McNutt and S. C. Sharma, J. Chem. Phys. **68**, 130 (1978).
[13]K. F. Canter and L. O. Roellig, Phys. Rev. A **12**, 386 (1975).
[14]S. C. Sharma (unpublished).
[15]B. N. Miller and T. L. Reese, Phys. Rev. A **39**, 4735 (1989).
[16]B. N. Miller, H. Lehtihet, J. M. Kowalski, and S. C. Sharma, J. Phys. B **22**, 1477 (1989).
[17]See, e.g., J. K. Percus, in *The Liquid State of Matter: Fluids Simple and Complex*, edited by F. W. Montroll and J. L. Leibowitz (North-Holland, Amsterdam, 1982), p. 31.
[18]J. M. Kowalski, S. C. Sharma, and B. N. Miller, in *Positron Annihilation Studies of Fluids*, edited by S. C. Sharma (World Scientific, Singapore, 1987), p. 368.
[19]R. L. Moore, Ph.D. thesis, Georgia Institute of Technology, 1979.
[20]R. K. Pathria, *Statistical Mechanics* (Pergamon, New York, 1972).
[21]B. A. Younglove and J. F. Ely, J. Phys. Chem. Ref. Data. **16**, 577 (1987).
[22]Y. Fan and B. N. Miller, Phys. Rev. B **41**, 4756 (1990).
[23]T. Silli, M. Tuomisaari, and R. M. Niemenen, in *Positron Annihilation*, edited by L. Dorikens-Vanpraet, M. Dorikens, and D. Segers (World Scientific, Singapore, 1989), p. 752.
[24]R. P. Feynman and A. R. Hibbs, *Quantum Mechanics and Path Integrals* (McGraw-Hill, New York, 1965); R. P. Feynman, Phys. Rev. **97**, 660 (1955).
[25]D. Chandler, Y. Singh, and D. M. Richardson, J. Chem. Phys. **81**, 1975 (1984); D. Chandler and P. Wolynes, *ibid.* **74**, 4078 (1981); A. L. Nichols III and D. Chandler, *ibid.* **81**, 5109 (1984).
[26]D. F. Coker and B. J. Berne, J. Chem. Phys. **86**, 5689 (1987).
[27]B. N. Miller and Y. Fan, Phys. Rev. A **42**, 2228 (1990).